APL Photonics

High-speed uni-traveling-carrier photodiodes on silicon nitride

Cite as: APL Photonics **8**, 016104 (2023); https://doi.org/10.1063/5.0119244
Submitted: 08 August 2022 • Accepted: 19 December 2022 • Accepted Manuscript Online: 19 December 2022 • Published Online: 13 January 2023

Dennis Maes, Sam Lemey, Gunther Roelkens, et al.

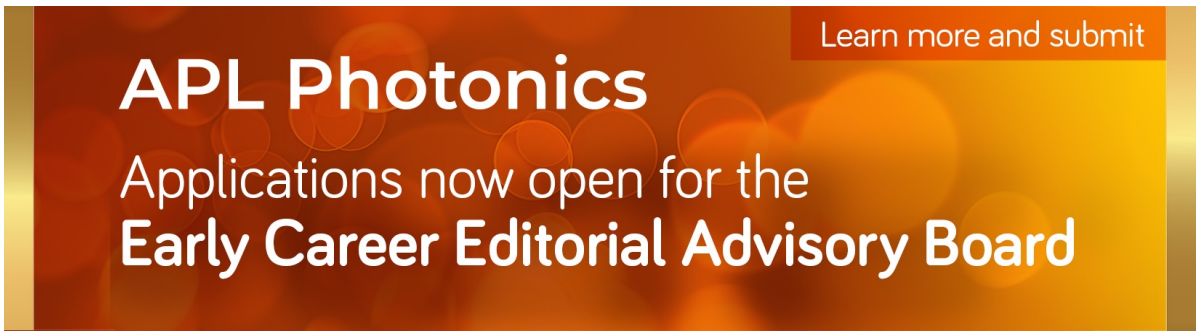

High-speed uni-traveling-carrier photodiodes on silicon nitride

Cite as: APL Photon. 8, 016104 (2023); doi: 10.1063/5.0119244
Submitted: 8 August 2022 • Accepted: 19 December 2022 •
Published Online: 13 January 2023

Dennis Maes,[1,2,3,a] Sam Lemey,[2] Gunther Roelkens,[1] Mohammed Zaknoune,[3] Vanessa Avramovic,[3] Etienne Okada,[3] Pascal Szriftgiser,[4] Emilien Peytavit,[3] Guillaume Ducournau,[3] and Bart Kuyken[1]

AFFILIATIONS

[1]Photonics Research Group, Department of Information Technology (INTEC), Ghent University—imec, Technologiepark-Zwijnaarde 126, 9052 Ghent, Belgium
[2]Internet Technology and Data Science Lab (IDLab), INTEC, Ghent University—imec, Technologiepark-Zwijnaarde 126, 9052 Ghent, Belgium
[3]Institut d'Electronique de Microélectronique et de Nanotechnologie (IEMN), CNRS–UMR 8520, Université de Lille, 59652 Villeneuve d'Ascq, France
[4]Laboratoire de Physique des Lasers Atomes et Molécules (PhLAM), CNRS–UMR 8523, Université de Lille, 59652 Villeneuve d'Ascq, France

[a]**Author to whom correspondence should be addressed:** dennis.maes@ugent.be

ABSTRACT

Integrated photonics is an emerging technology for many existing and future telecommunication and data communication applications. One platform of particular interest is silicon nitride (SiN), thanks to—among others—its very low-loss waveguides. However, it lacks active devices, such as lasers, amplifiers, and photodiodes. For this, hybrid or heterogeneous integration is needed. Here, we bring high-speed uni-traveling-carrier photodiodes to a low-loss SiN-platform by means of micro-transfer-printing. This versatile technology for heterogeneous integration not only allows very dense and material-efficient III–V integration but also eases the fabrication, yielding high-performance detectors. The waveguide-coupled photodiodes feature a responsivity of 0.3 A/W at 1550 nm, a dark current of 10 nA, and a bandwidth of 155 GHz at a low bias. At zero bias, a record bandwidth of 135 GHz is achieved. We further demonstrate that this integrated detector can be used for direct photomixing at terahertz frequencies. A back-to-back communication link with a carrier frequency of around 300 GHz is set up, and data rates up to 160 Gbit/s with a low error vector magnitude are shown, showcasing a near-identical performance at zero bias.

I. INTRODUCTION

Integrated photonic solutions are key to solve many challenges for next-generation telecommunication, LIDAR, and quantum computing systems. More specifically, silicon nitride (SiN) platforms prevail over other materials, thanks to the very low-loss waveguides and some of the best integrated filters.[1] Unfortunately, active devices are not natively available. In recent years, the heterogeneous integration of amplifiers and lasers has been demonstrated.[2,3] However, for communication—be it telecom, datacom, or microwave photonics—the compact integration of high-speed detectors is even more important.

The widespread adoption of SiN platforms is held back by the absence of such high-bandwidth photodiodes. Table I shows a comparison of the state-of-the-art waveguide-coupled photodetectors at 1550 nm for different material platforms. Germanium on silicon[4] (Ge-on-Si) currently offers some of the best waveguide-coupled photodiodes for photonic integration, although this solution is not transferable to low-loss SiN platforms. A Ge-on-Si photodiode coupled to a SiN waveguide is demonstrated at O-band[8] but uses plasma-enhanced chemical vapor deposition (PECVD) of SiN. For true low-loss waveguides at C-band, low pressure chemical vapor deposition (LPCVD) of SiN is required. Monolithic III–V photodiodes[5,6]—often uni-traveling-carrier photodiodes (UTC PDs)—also show very high bandwidths, but these lossy waveguide platforms are not suitable for large scale photonic integration. On the other hand, the current solutions to bring III–V photodiodes to SiN show only limited bandwidths. So far, wafer bonding has

TABLE I. State of the art of waveguide-coupled photodetectors at 1550 nm.

Platform[Ref.]	Responsivity (A/W)	Bandwidth (GHz)	Bandwidth at zero bias (GHz)
Ge-on-Si, monolithic[4]	0.30	265	>67[a]
III–V, monolithic[5]	0.36	108	3
III–V, monolithic[6]	0.48	100	66
III–V on SiN, bonded[7]	0.80	20	...
III–V on SiN, transfer-printed (this work)	0.30	155	135

[a]For photocurrents above 1 mA this drops below 67 GHz.

held the highest record with a bandwidth of 20 GHz.[7] Although wafer bonding can potentially reach an identical performance, it lacks the versatility of micro-transfer-printing that allows native source-wafer processing, heterogeneous integration of multiple material sources, and Back-End-Of-Line (BEOL) integration on non-flat surfaces (e.g., a local recess in the top cladding).

We demonstrate a UTC PD heterogeneously integrated on a SiN photonics platform with a bandwidth of over 100 GHz, even at zero bias. This high-bandwidth bias-free operation additionally paves the way for future mmWave and terahertz wireless technologies such as on-chip remote antenna units (RAUs) that are not possible with existing platforms. For a phased antenna array to support grating-lobe-free beam steering, strict requirements are imposed on the spacing in between antenna elements and, thus, on the space available for photodiode integration. The bias-free operation eliminates the need for a DC-feed network that often cannot be sufficiently miniaturized.

To showcase the performance of our heterogeneous integration approach, we demonstrate a communication link at 300 GHz with data rates up to 160 Gbit/s. These are, to the best of our knowledge, the first 100 Gbit/s signals and beyond using bias-free optical-to-THz converters.

II. DESIGN AND FABRICATION

The UTC PDs are integrated on SiN waveguides by means of micro transfer-printing[9] (Fig. 1). First, pickable chiplets—coupons—are made on a III–V source wafer and then transfer-printed to the SiN target chip, as demonstrated earlier.[9]

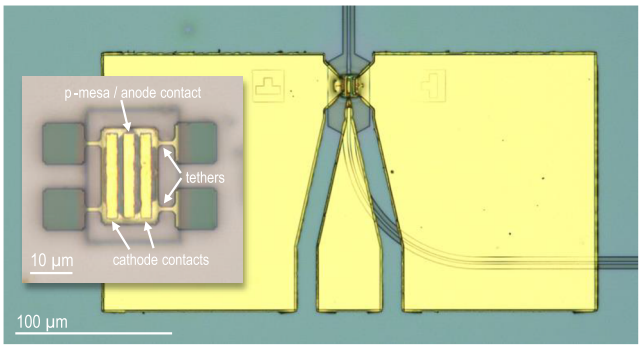

FIG. 1. A uni-traveling-carrier photodiode (UTC PD) is integrated on a SiN platform by transfer-printing a coupon (inset) on a waveguide.

The design of the epitaxial layer stack is based on the work of Latzel *et al.*[10] and adapted to the micro-transfer-printing process (see Table II). This boils down to including a 500 nm release layer between the InP substrate and the functional layers. To reduce the dishing effect of an under-etch, $In_{0.52}Al_{0.48}As$ is chosen as the material for this sacrificial release layer.[11] Compared to InGaAs, it is etched isotropically and, thus, faster. This ensures that the bottom surface of the coupon is flat. The UTC epitaxial layer stack features an undoped collector of 100 nm and a 150 nm-thick absorption region with a graded composition. This results in a graded bandgap that improves the electron transport in the absorption layer by boosting the built-in electric field.

The design of the individual waveguide photodiodes consists of a central mesa, the active layer of the photodiode that contains the absorbing and collecting layer, as well as the anode contact on top. This mesa is flanked by two cathode contacts, separated only 500 nm apart, to allow the wider base of the mesa caused by its slanted sidewalls. Electromagnetic simulations, including 3D finite-difference time-domain (FDTD) simulations, show a waveguide (mesa) width of 2 µm to be ideal in terms of mode coupling efficiency and overall absorption, as well as tolerance for transfer-printing alignment. Introducing a taper in the non-absorbing InP sub-contact layer might reduce the reflections at the high index contact transition. However, eigenmode expansion (EME) propagation simulations showed little to no improvement in the amount of light reflected if a taper were introduced. The simulations showed that by intelligently choosing the waveguide width and coupon separation, reflections are very low. The simulations of the optimized design show reflections below 1%. Photodiodes with three different waveguide lengths (12, 16, and 20 µm) were designed as a trade-off between the absorption length and increased junction capacitance. From simulations, it is expected that already more than 80% of the optical power is absorbed after 12 µm, and over 90% at 16 µm.

The UTC PD is made entirely on a III–V source wafer [Fig. 2(a)]. This process includes two metal depositions for anode and cathode contacts. The metal stack consists of 10 nm Ti, promoting the adhesion to the InGaAs layers, as well as 40 nm Pt, to prevent diffusion of the top Au layer. A self-aligned 2 µm-wide waveguide mesa is etched down to the cathode contact layer, followed by a device etch down to the release layer using a SiN hard mask [Fig. 2(b)].

To make transfer-printing possible, these diodes need to be converted into diode coupons, i.e., pickable chiplets. To do so, the release layer is first etched anisotropically with a padding of a few micrometer around the diode. A SiN encapsulation layer is deposited, and tethers that support the diode are patterned and etched within. The thickness of this layer is 500 nm, which yields a layer strong enough to support the coupon but still weak enough to break during the pick-up step of transfer-printing. Finally, the remainder of the InAlAs release layer is underetched isotropically using a chilled $FeCl_3$ solution, resulting in a suspended coupon [Fig. 2(c)].

Next, a photonic integrated circuit (PIC) was designed and fabricated on a SiN platform using in-house e-beam lithography. The material stack of the silicon target wafer consists of 3.3 µm-thick buried oxide (BOX) and 300 nm-thick SiN [Fig. 2(e)]. The

TABLE II. UTC epitaxial layer stack.

Feature	Material	T (nm)	Doping (cm^{-3})
Anode contact	$In_{0.4}Ga_{0.6}As$	10	$p = 1 \times 10^{20}$
Diffusion barrier	$Al_{0.075}In_{0.53}Ga_{0.395}As$	20	$p = 5 \times 10^{19}$
Absorption region	$In_{0.47}Ga_{0.53}As$ to $In_{0.4}Ga_{0.6}As$[a]	150	$p = 1 \times 10^{18}$
Spacer	$Al_{0.235}In_{0.53}Ga_{0.235}As$	20	n.i.d.
Cliff layer	InP	7	$n = 1 \times 10^{18}$
Collector region	InP	100	n.i.d.
Sub-collector	InP	50	$n = 3 \times 10^{19}$
Cathode contact	$In_{0.4}Ga_{0.6}As$	10	$n = 3 \times 10^{19}$
Sub-contact	InP	300	$n = 3 \times 10^{19}$
Etch stop	$In_{0.4}Ga_{0.6}As$	20	$n = 3 \times 10^{19}$
Release layer	$In_{0.52}Al_{0.48}As$	500	$n = 1 \times 10^{18}$
Buffer	InP	17.5	n.i.d.

[a]Graded composition.

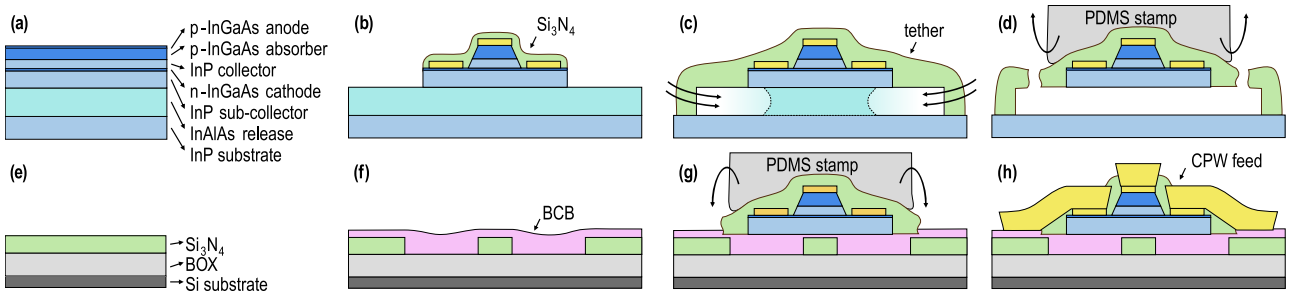

FIG. 2. Fabrication flow: (a) epitaxial growth of the source III–V wafer. (b) Creation of a diode by etching the mesa, deposition of anode and cathode contacts, and SiN passivation. (c) After tethering the diode to the substrate with a new of layer SiN, the release layer is etched away. (d) This suspended coupon is then picked up by a polydimethylsiloxane (PDMS) stamp of the micro-transfer-printer. (e) The silicon target wafer with 300 nm SiN on top of the BOX. (f) Waveguides are created, and a thin layer of benzocyclobutene (BCB) is spin-coated. (g) The coupon is then printed on top of the waveguide and (h) post-processed to create electrical contacts.

design features an array of simple printing sites. For easy coupling, each photodiode is fed by a 0.5 mm long waveguide connected to a focused grating coupler. A thin layer of benzocyclobutene (BCB) is spin-coated on the sample, which makes the adhesion better during transfer-printing and fixates the coupon after curing [Fig. 2(f)].

The coupon is then transfer-printed by picking it up from the source wafer [Fig. 2(d)] and printing it on the target wafer [Fig. 2(g)] using a dedicated flexible stamp, made out of polydimethylsiloxane (PDMS). As a final step after transfer-printing, vias are etched in the SiN-layer and a coplanar waveguide (CPW) of 100 μm is deposited. This allows us to probe the photodiode electrically.

III. RESULTS

A. Performance

1. Passives

The SiN waveguides were verified to have losses below 1 dB/cm. Although this is still very low, waveguide etching in an industrial cleanroom (as compared to our research-grade tools) and only applying the BCB adhesion layer on a limited section of the waveguides (by locally opening up the top cladding layer) would further improve this. The grating couplers show an insertion loss of 9 dB at 1550 nm. These high losses can be attributed to the design of this coupler, as well as the BCB layer, which shifts the coupler's central wavelength away from 1550 nm. As the grating coupler is not an intrinsic part of the photodetector and coupling losses could easily be lowered using an edge coupler, we will, from now on, consider the on-chip power.

2. Responsivity

The responsivity of the photodiodes at a wavelength of 1550 nm is measured to be 0.3 A/W. This responsivity was verified to be constant for bias voltages ranging between −2.5 and 0 V, as well at low and high power levels, up to multiple milliwatts on-chip power. This results in a (waveguide-referenced) external quantum efficiency (EQE) of 23%.

Although photodiodes with different waveguide lengths—12, 16, and 20 μm—were made, no significant correlation with an increased responsivity is found. It is believed that the excess light is absorbed in areas not contributing to the photocurrent,

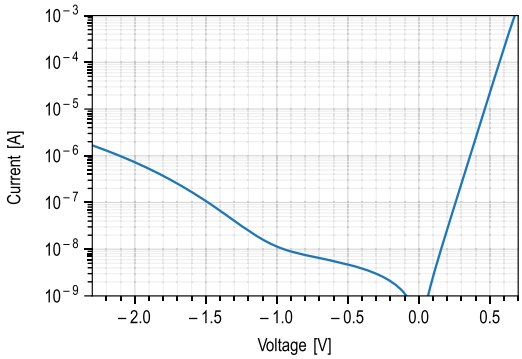

FIG. 3. The dark current for a PD with a 2 × 16 μm^2 active area is below 10 nA for a bias voltage above −1 V.

such as the metal contacts. Hence, increasing the length of the waveguide-coupled UTC PD is not beneficial.

3. Dark current

The dark current equals to 10 and 5 nA at −1.0 and −0.5 V biases, respectively. Two clear distinct regions in the dark current response can be observed in Fig. 3: a relatively flat region down to −1 V bias, and a strong increase beyond −1 V bias. In the former region, the Shockley–Read–Hall (SRH) recombination, assisted by traps, is the main contribution to the dark current, whereas in the latter, band-to-band tunneling is dominating.[12] We believe the dark current density, which is in the order of magnitude of 1 mA/cm^2, can be attributed to the surface leakage current caused by the mesa sidewall passivation.

4. Saturation

The 1 dB saturation point is reached at 4.6 mA photocurrent for −1 V bias with a RF power output of −4.1 dBm at 100 GHz as shown in Fig. 4. This is also very close to the thermal breakdown current. At zero bias, the saturation is reached at 2.8 mA with an output power of −9.7 dBm at 100 GHz. The effective resistance r_{eff}, given by P_{RF}/I^2_{phot}, serves as a good measure for the photocurrent to RF conversion efficiency, independent of the optical power.[10] These diodes show a high efficiency with r_{eff} going up to 20 Ω.

5. Impedance

The impedance of the photodiodes was measured with a vector network analyzer (VNA) up to 67 GHz. After de-embedding the results with a basic open–short calibration, a very good fit ($R^2 > 0.99$) with a series RC circuit could be made. It showed a junction capacitance of 18.5, 25, and 31 fF for PDs with a length of 12, 16, and 20 μm, respectively. This is a unit capacitance of 0.8 fF/μm^2, slightly below the expected 1 fF/μm^2 for an InP collector of 100 nm. At zero-bias, the junction capacitance is about 10% higher. The series resistance is very low, varying between 4 and 10 Ω.

6. Frequency response

The frequency response of the photodiodes was measured using a set of power detectors. The lower frequency range (0–110 GHz) was measured using a coaxial probe, bias-tee, and thermal power meter (R&S NRP-Z58). The higher frequency ranges were measured with a calorimeter-style power meter (Erickson PM5) and two waveguide probes with an integrated bias-tee: a WR5-probe (140–220 GHz) and a WR3-probe (220–325 GHz). The results were corrected for probe, bias-tee, and THz-waveguide losses, as provided in the datasheets of the suppliers.

A photodiode with an active area of 2 × 12 μm^2 showed a 3-dB bandwidth of 155 GHz at −1 V bias, which is faster than any state-of-the-art photodiode heterogeneously integrated on SiN.[7,10] At zero bias, a bandwidth of 135 GHz is obtained, which is even higher than the best silicon-on-insulator (SOI) counterparts.[4] It should be noted that the 135 GHz-bandwidth is based on the interpolated data, as can be seen in the normalized frequency response (Fig. 5).

Due to the thin layer thickness and high electron mobility in the absorption region, the bandwidth is mostly limited by the RC time constant (f_{RC}).[13] If we take into account the extracted junction capacitance C_j of 18.5 fF, the series resistance R_s of 4 Ω, and the 50 Ω impedance of the measurement equipment, the calculated f_{RC} equals 159 GHz. The transit-time cut-off frequency (f_{TT}) is calculated to be 424 GHz for an estimated electron drift velocity of 3.5 × 10^7 cm/s in the 150-nm thick absorber. This results in an overall 3-dB bandwidth of 146 GHz, which is very close to the measured result. This small difference is attributed to the uncertainty on the effective electron

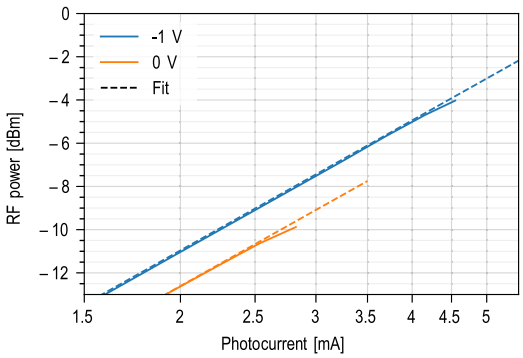

FIG. 4. RF power at 100 GHz. The 1 dB saturation current for a PD with a 2 × 16 μm^2 active area is above 4.6 mA at −1 V bias and 2.8 mA at zero bias.

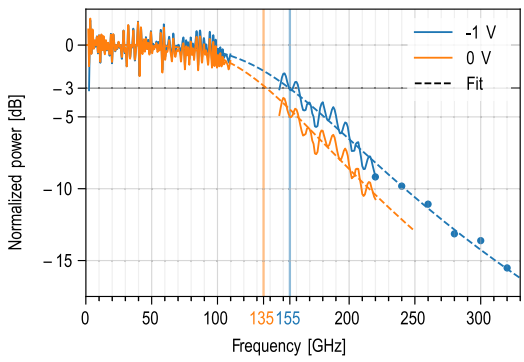

FIG. 5. The 3-dB bandwidth for a PD with a 2 × 12 μm^2 active area is 155 GHz at −1 V bias and 135 GHz at zero bias, both with a photocurrent of 1 mA.

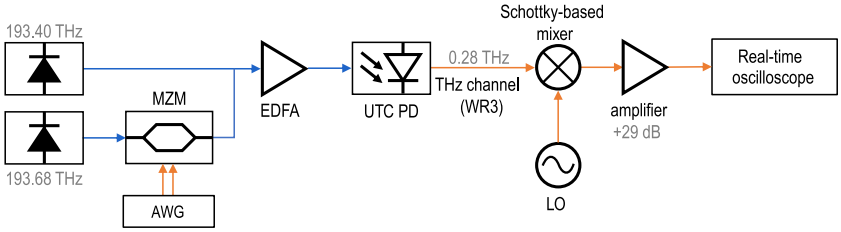

FIG. 6. In this experimental setup, two separate lasers are used for photomixing. One line is modulated using a MZM, before being combined and amplified by an EDFA. The light is coupled into the PIC using a vertical grating coupler, and the mixed terahertz signal is then transferred over a WR3 waveguide channel before down-mixing, post-amplification, and sampling.

velocity in the absorber and the possible inductive effects of the CPW contacts. At zero bias, the calculated RC-limit is 145 GHz, implying a small additional decrease in the transit-time bandwidth as well.

B. Terahertz communication experiment

To demonstrate the capabilities of this photodiode at terahertz frequencies, a data experiment with a carrier frequency of around 300 GHz is set up (Fig. 6). Two C-band laser lines, of which one is modulated by a Mach–Zehnder modulator (MZM), are combined and fed in the photonic integrated circuit (PIC). The mixed terahertz signal is then coupled out of the PIC by a ground–signal–ground (GSG) probe. Here, no electrical mixers at the transmit side are used and photomixing directly happens in the photodiode. This signal is then transmitted back-to-back (B2B), i.e., over a short WR-3 waveguide channel without additional attenuation. At the receiver side, the terahertz signal is down-converted using a Schottky-based diode mixer, post-amplified by 29 dB, and sampled by a real-time oscilloscope. A linear equalizer compensates for the dispersion introduced by the Schottky-based mixer: both its deterministic RF response and IF frequency dependence are compensated for. However, no pre-compensation is applied at the transmit side. Hence, the remaining distortion is due to the uncompensated roll-off behavior of the UTC-PD at around 280 GHz.

The performance of this THz-link was verified, and data rates beyond 100 Gbit/s were achieved with low error vector magnitudes (EVMs). All further values for the EVM are referenced to the peak constellation power. These high data rates were achieved using multiple combinations of constellation formats, e.g., 16-point quadrature amplitude modulation (16-QAM) at 35 GBd (140 Gbit/s) and 32-QAM at 25 GBd (125 Gbit/s). An optical input of 11 dBm was used, resulting in a photocurrent of 2.80 mA and RF-power of about −20 dBm (10 μW) at −1 V bias. At zero bias, the photocurrent is 2.65 mA, which is slightly lower due to the reduced bandwidth. As shown in Fig. 7, a low EVM was achieved with a very small penalty for the absence of a bias voltage (zero bias). When using 16-QAM at 35 GBd (−1 V), the EVM rises by 0.7%, from 11.2% to 11.9%.

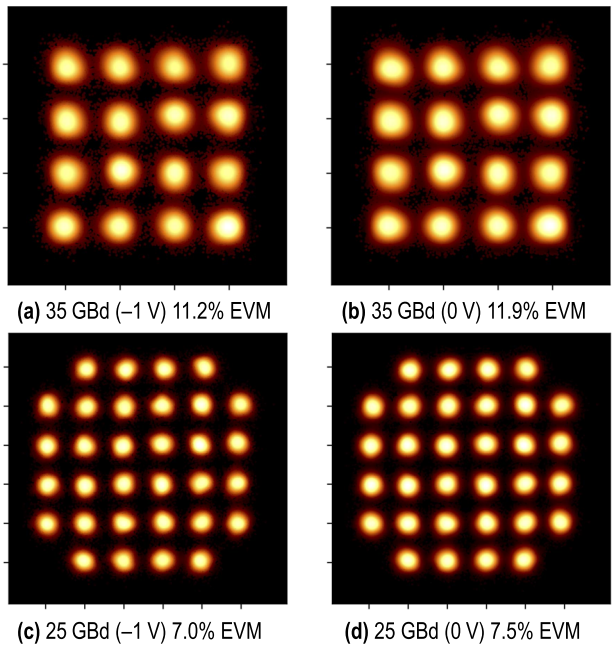

FIG. 7. A clear distinction between constellation points is visible at high data rates of 140 Gbit/s [(a) and (b)] and 125 Gbit/s [(c) and (d)], with a very small difference between −1 and 0 V biases. (a) 16-QAM at 35 GBd (−1 V) with an EVM of 11.2%. (b) 16-QAM at 35 GBd (0 V) with an EVM of 11.9%. (c) 32-QAM at 25 GBd (−1 V) with an EVM of 7.0%. (d) 32-QAM at 25 GBd (0 V) with an EVM of 7.5%.

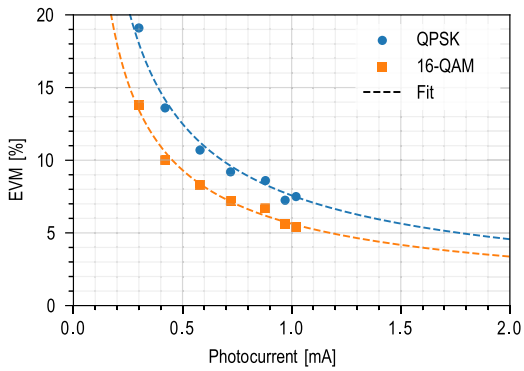

FIG. 8. The EVM for a 4 GBd transmission shows a clear inversely-quadratic fit with no deterioration for increased photocurrents.

Meanwhile, when using 32-QAM at 25 GBd (−1 V), the EVM only increased by 0.5%, from 7.0% to 7.5%.

A second series of experiments was performed to asses the influence of the photocurrent level on the EVM. For a consistent result, this was done at a lower symbol rate of 4 GBd to avoid any influence of other bandwidth limiting devices in the setup. Figure 8 shows the EVM for a 4 GBd transmission. The photocurrent is limited to 1 mA as this was the maximal photocurrent achievable with the Thorlabs EDFA100P erbium-doped fiber amplifier (EDFA), which showed lower noise levels than the higher-powered Manlight EDFA. For an increased power, the EVM decreases according to an inversely-quadratic fit. This demonstrates that the EVM is noise limited and no linearity effects occur at 1 mA.

IV. CONCLUSION

Waveguide-coupled UTC photodiodes can be integrated on a SiN-platform by means of micro-transfer-printing. This approach allows for the separate fabrication of the III–V chiplet and SiN PIC, ensures an efficient material usage, and delivers high-performance waveguide-coupled photodetectors. The demonstrated UTC PDs show a responsivity of 0.3 A/W, a low dark current below 10 nA (> −1 V bias), high bandwidths of 155 GHz at −1 V bias and 135 GHz at zero bias, and a saturation current of above 4.5 mA. We have showcased that this device can be used at terahertz frequencies (300 GHz) and supports data rates beyond 100 Gbit/s with a low EVM. To the best of our knowledge, this is the fastest photodiode on SiN and the fastest zero-bias photodiode cross-platform.

AUTHOR DECLARATIONS

Conflict of Interest

The authors have no conflicts to disclose.

Author Contributions

Dennis Maes: Conceptualization (lead); Data curation (lead); Formal analysis (lead); Investigation (lead); Methodology (lead); Software (lead); Validation (lead); Visualization (lead); Writing – original draft (lead); Writing – review & editing (lead). **Sam Lemey**: Funding acquisition (equal); Supervision (equal); Writing – review & editing (equal). **Gunther Roelkens**: Supervision (supporting); Writing – review & editing (equal). **Mohammed Zaknoune**: Methodology (supporting); Writing – review & editing (supporting). **Vanessa Avramovic**: Methodology (supporting). **Etienne Okada**: Methodology (supporting). **Pascal Szriftgiser**: Methodology (supporting). **Emilien Peytavit**: Investigation (equal); Methodology (equal); Writing – review & editing (supporting). **Guillaume Ducournau**: Investigation (equal); Methodology (equal); Writing – review & editing (supporting). **Bart Kuyken**: Funding acquisition (equal); Supervision (equal); Writing – review & editing (equal).

DATA AVAILABILITY

The data that support the findings of this study are available from the corresponding author upon reasonable request.

REFERENCES

[1] T. J. Kippenberg, A. L. Gaeta, M. Lipson, and M. L. Gorodetsky, "Dissipative Kerr solitons in optical microresonators," Science **361**, eaan8083 (2018).
[2] C. Xiang, J. Guo, W. Jin, L. Wu, J. Peters, W. Xie, L. Chang, B. Shen, H. Wang, Q.-F. Yang, D. Kinghorn, M. Paniccia, K. J. Vahala, P. A. Morton, and J. E. Bowers, "High-performance lasers for fully integrated silicon nitride photonics," Nat. Commun. **12**, 6650 (2021).
[3] C. Op de Beeck, B. Haq, L. Elsinger, A. Gocalinska, E. Pelucchi, B. Corbett, G. Roelkens, and B. Kuyken, "Heterogeneous III-V on silicon nitride amplifiers and lasers via microtransfer printing," Optica **7**, 386–393 (2020).
[4] S. Lischke, A. Peczek, J. S. Morgan, K. Sun, D. Steckler, Y. Yamamoto, F. Korndörfer, C. Mai, S. Marschmeyer, M. Fraschke, A. Krüger, A. Beling, and L. Zimmermann, "Ultra-fast germanium photodiode with 3-dB bandwidth of 265 GHz," Nat. Photonics **15**, 925–931 (2021).
[5] E. Rouvalis, C. C. Renaud, D. G. Moodie, M. J. Robertson, and A. J. Seeds, "Traveling-wave uni-traveling carrier photodiodes for continuous wave THz generation," Opt. Express **18**, 11105–11110 (2010).
[6] F. Yu, K. Sun, Q. Yu, and A. Beling, "High-speed evanescently-coupled waveguide type-II MUTC photodiodes for zero-bias operation," J. Lightwave Technol. **38**, 6827–6832 (2020).
[7] Q. Yu, J. Gao, N. Ye, B. Chen, K. Sun, L. Xie, K. Srinivasan, M. Zervas, G. Navickaite, M. Geiselmann, and A. Beling, "Heterogeneous photodiodes on silicon nitride waveguides," Opt. Express **28**, 14824 (2020).
[8] S. Lischke, D. Knoll, C. Mai, A. Hesse, G. Georgieva, A. Peczek, A. Kroh, M. Lisker, D. Schmidt, M. Fraschke, H. Richter, A. Krüger, U. Saarow, P. Heinrich, G. Winzer, K. Schulz, P. Kulse, A. Trusch, and L. Zimmermann, "Silicon nitride waveguide coupled 67+ GHz Ge photodiode for non-SOI PIC and ePIC platforms," in *2019 IEEE International Electron Devices Meeting (IEDM)* (IEEE, 2019), pp. 33.2.1–33.2.4.
[9] D. Maes, G. Roelkens, M. Zaknoune, C. O. de Beeck, S. Poelman, M. Billet, M. Muneeb, S. Lemey, E. Peytavit, and B. Kuyken, "Heterogeneous integration of uni-travelling-carrier photodiodes using micro-transfer-printing on a silicon-nitride platform," in *2021 Conference on Lasers and Electro-Optics Europe and European Quantum Electronics Conference* (Optica Publishing Group, 2021), p. ck_4_3.
[10] P. Latzel, F. Pavanello, M. Billet, S. Bretin, A. Beck, M. Vanwolleghem, C. Coinon, X. Wallart, E. Peytavit, G. Ducournau, M. Zaknoune, and J.-F. Lampin, "Generation of mW level in the 300-GHz band using resonant-cavity-enhanced unitraveling carrier photodiodes," IEEE Trans. Terahertz Sci. Technol. **7**, 800–807 (2017).
[11] J. O'Callaghan, R. Loi, E. E. Mura, B. Roycroft, A. J. Trindade, K. Thomas, A. Gocalinska, E. Pelucchi, J. Zhang, G. Roelkens, C. A. Bower, and B. Corbett, "Comparison of InGaAs and InAlAs sacrificial layers for release of InP-based devices," Opt. Mater. Express **7**, 4408–4414 (2017).
[12] M. Verdun, G. Beaudoin, B. Portier, N. Bardou, C. Dupuis, I. Sagnes, R. Haïdar, F. Pardo, and J.-L. Pelouard, "Dark current investigation in thin P-i-N InGaAs photodiodes for nano-resonators," J. Appl. Phys. **120**, 084501 (2016).
[13] M. N. Feiginov, "Analysis of limitations of terahertz p-i-n uni-traveling-carrier photodiodes," J. Appl. Phys. **102**, 084510 (2007).